Deterministic cavity quantum electrodynamics with trapped ions

Article (Unspecified)

INSTITUTE OF PHYSICS PUBLISHING JOURNAL OF PHYSICS B: ATOMIC, MOLECULAR AND OPTICAL PHYSICS

J. Phys. B: At. Mol. Opt. Phys. **36** (2003) 613–622 PII: S0953-4075(03)54731-9

Deterministic cavity quantum electrodynamics with trapped ions

M Keller[1], B Lange[1], K Hayasaka[2], W Lange[1] and H Walther[1]

[1] Max-Planck-Institut für Quantenoptik, Hans-Kopfermann-Str 1, 85748 Garching, Germany
[2] Communications Research Laboratory, 588-2 Iwaoka, Nishi-ku, Kobe 651-2492, Japan

E-mail: wfl@mpq.mpg.de

Received 11 October 2002
Published 27 January 2003
Online at stacks.iop.org/JPhysB/36/613

Abstract

We have employed radio-frequency trapping to localize a single $^{40}Ca^{+}$-ion in a high-finesse optical cavity. By means of laser Doppler cooling, the position spread of the ion's wavefunction along the cavity axis was reduced to 42 nm, a fraction of the resonance wavelength of ionized calcium ($\lambda = 397$ nm). By controlling the position of the ion in the optical field, continuous and completely deterministic coupling of ion and field was realized. The precise three-dimensional location of the ion in the cavity was measured by observing the fluorescent light emitted upon excitation in the cavity field. The single-ion system is ideally suited to implement cavity quantum electrodynamics under cw conditions. To this end we operate the cavity on the $D_{3/2}$–$P_{1/2}$ transition of $^{40}Ca^{+}$ ($\lambda = 866$ nm). Applications include the controlled generation of single-photon pulses with high efficiency and two-ion quantum gates.

1. Introduction

The concept of coupling a single atom to a single mode of the electromagnetic field is the basis of cavity quantum electrodynamics (CQED), an area which has produced impressive advances in the experimental investigation of the interaction between matter and quantized radiation fields [1]. The most relevant regime for observing quantum phenomena of the atom–field dynamics is reached when the strength of the atom–field coupling exceeds the effects of spontaneous emission and damping of the cavity field. In this case, the coherent exchange of excitation between atom and photon is the dominating process.

Strong coupling has been achieved in two different spectral domains: at *microwave frequencies*, a beam of highly excited Rydberg atoms is coupled to the field of a superconducting microwave cavity with a very high Q-factor [2, 3]. The large dipole matrix elements of Rydberg transitions, combined with long radiative lifetimes and low ohmic losses of the cavity

0953-4075/03/030613+10$30.00

field, lead to a strong coherent coupling of atoms and microwave radiation. Fields with non-classical properties are built up when a sequence of atoms traverses the cavity with suitable interaction times. A drawback of Rydberg atom systems is the lack of detectors for single microwave photons, precluding the direct observation of the quantized field. Measurements on the system are restricted to the state of the atoms exiting the cavity.

Strong coupling in the *optical regime* has been reached using cavities with small mode-volume. In this case, the rate of coherent interaction between atoms and field may exceed the atomic spontaneous emission rate. Damping of the field is minimized by employing mirrors with ultra-low losses. In contrast to the microwave case, the radiation leaking from the cavity can be detected with single-photon counters, or it can be used in successive experiments. A signature observation in this regime is the splitting of the normal modes of the combined atom–cavity system as a result of the interaction between atom and vacuum field [4, 5].

The properties of CQED systems make strongly coupled atoms and photons prime candidates for quantum information processing [6]. The objective is to use the quantum evolution of the system to perform computation in a more efficient way than a classical computer. Not surprisingly, one of the first realizations of conditional quantum dynamics was achieved with caesium atoms traversing an optical cavity [7], laying the foundation for a quantum logic gate. The interaction of atoms and the optical cavity field provides an interface between atomic and photonic degrees of freedom, which is an essential component for the long-distance coupling of local quantum information processing sites [8, 9].

In a cavity, the coupling g between atom and field varies with the local field strength at the position of the atom. Its distribution is characterized by a standing-wave structure along the cavity axis and exponentially decreasing transverse modes. This poses a problem when non-stationary atoms are used, as was the case in all previous experiments in optical CQED. At *microwave frequencies*, the problem is less severe, because cavities are operated in fundamental modes with little intensity variation over the transverse size of the atomic beam. By contrast, in experiments at *optical frequencies*, there is no control of atomic trajectories at the scale of typical cavity-field structures, which for a standing wave is given by half the transition wavelength. Interaction with the field at a definite atomic position can only be obtained post-selectively by evaluating information obtained from the photons leaking from the cavity. This method was employed recently to reconstruct the trajectories of single atoms in a cavity [10, 11]. Quantum computation, however, requires the deterministic control of the interaction of the quantum bits, which cannot be implemented if the atoms experience a random coupling with the field during their flight through the cavity.

To use optical CQED systems for quantum information processing, the most important task is to permanently localize atoms in the cavity on a scale set by the wavelength of the radiation (Lamb–Dicke localization). The required degree of confinement is provided routinely in radio-frequency (rf) ion traps [12]. We have recently employed a linear trap to localize a single calcium ion in an optical cavity [13]. This paper describes the principal experimental techniques we use in the realization of a CQED system with trapped ions (section 2). A figure of merit is the three-dimensional extension of the ion's wavepacket compared with the characteristic size of the spatial field structure in the cavity. We have probed the localization of the calcium ion in the cavity by using it as a near-field detector of the local cavity intensity, demonstrating a well-defined atom–cavity coupling on a sub-wavelength scale (section 3). The deterministic control of the system dynamics achieved in our system has a number of applications based on the coherent manipulation of atom–photon systems at the single-quantum level. Two examples are discussed in section 4: the generation of triggered single-photon pulses and the entanglement of two ions interacting with the cavity mode.

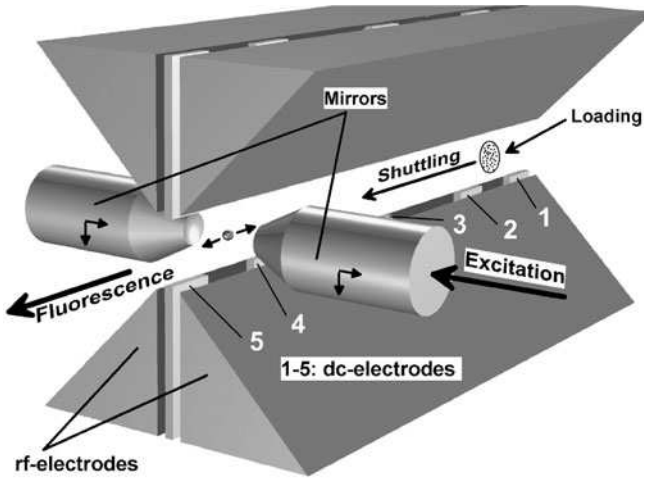

Figure 1. Setup of the single-ion CQED system used in the experiment. The loading zone and the cavity interaction region are located at opposite ends of the linear trap. The rf electrodes are shaped to provide optimum side access for laser beams and placement of the cavity mirrors.

2. Experimental techniques

In our CQED system we use a single calcium ion stored in a trap with linear geometry, as shown in figure 1. Radial confinement is provided by applying a rf voltage of 400 V at 12.7 MHz to the four electrodes in a quadrupole mass-filter arrangement, resulting in a harmonic pseudopotential with an oscillation frequency of 1.3 MHz. In the axial direction, the position of the ion is controlled with five pairs of electrodes, located in the vertical gap between the rf electrodes. By applying a dc voltage of 20 V to the outer sets of electrodes (1, 2 and 4, 5 in figure 1), harmonic axial confinement at a frequency of 300 kHz is achieved.

The linear geometry allows us to spatially separate the cavity zone and the loading region. This is necessary to avoid the detrimental effects of the loading process on the cavity-mirrors. Ions are generated either by electron-impact ionization or by photo-ionization of an atomic calcium beam. In the first case, loading in the vicinity of the mirrors would expose them to charging by the electron beam, leading to unstable trapping conditions. In addition, coating of the mirror surface with calcium would result in absorption losses of the cavity field. Both problems are avoided by loading the ions at a distance of 23 mm from the cavity zone (between the rear electrodes 1 and 2 in figure 1). The most efficient method to produce ions is photo-ionization [14, 15]. In the case of calcium we use a laser at 423 nm to excite the $4p\ ^1P_1$ state and a laser at 390 nm to populate a Rydberg level, which then ionizes in the trapping field.

Subsequently, the ions are shuttled to the cavity zone. To this end, all dc-electrodes except the outer pairs are grounded, so that the ions are free to move between electrodes 1 and 5. By successively ramping the voltages at electrodes 1, 2 and 3 to 400 V, the ions are pushed towards the cavity region, reaching their equilibrium position at the centre of the cavity after electrode 4 is set to 20 V. Snapshots of the axial potential during the transfer process are shown in figure 2. The entire sequence is completed in 4 ms.

The $^{40}Ca^+$ ion was chosen because its level scheme (shown in figure 3) is ideally suited for implementing CQED with ions. The Λ system formed by the $S_{1/2}$ ground state, the $P_{1/2}$ excited state and the metastable $D_{3/2}$ state provides two electric dipole transitions. The resonance transition $S_{1/2} \rightarrow P_{1/2}$ at 397 nm is not suited for coherent coupling to a cavity,

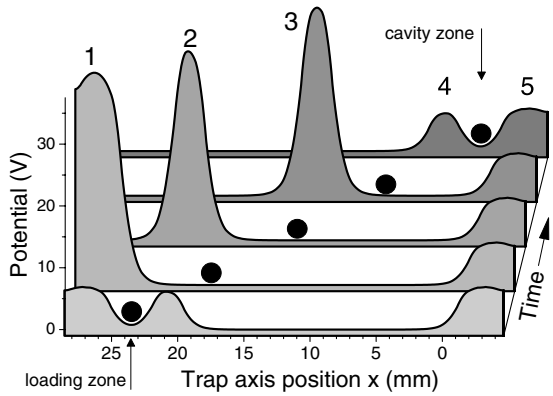

Figure 2. Sequence of axial potential distributions used to shuttle the ion from the loading to the cavity zone, obtained from a three-dimensional finite-element calculation. The black circle indicates the position of the ion, the electrode numbers correspond to those in figure 1.

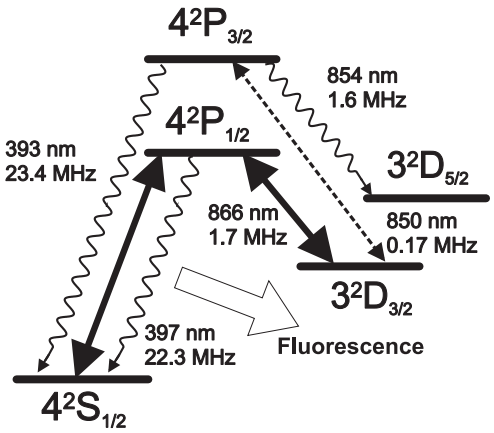

Figure 3. Level scheme of $^{40}Ca^{+}$, indicating the wavelength and linewidth of transitions relevant for CQED. Cavity and pump laser are represented by solid lines. The dashed transition is used for repumping and the observation of quantum jumps.

because scattering and absorption losses in the mirror coatings are prohibitively large in the ultraviolet region (the mirrors we have tested had losses of more than 1000 ppm). The 397 nm line is used for Doppler cooling the ion's external degrees of freedom. The angle at which the laser beam is injected is chosen to provide cooling along all the principal axes of the trap. By observing the emitted fluorescent light, the ion is detected and diagnosed.

The transition $D_{3/2} \rightarrow P_{1/2}$ at 866 nm is in a spectral region where mirror losses as low as a few parts per million are obtained [16, 17]. Therefore, this transition is used for coupling the ion to the cavity. For applications in quantum information processing, it is desirable to couple the cavity field to a pair of long-lived electronic states. In $^{40}Ca^{+}$, the $S_{1/2}$ ground state and the $D_{3/2}$ metastable state are most suitable. They may be coupled to the cavity field by means of an off-resonant Raman transition driven by a laser at 397 nm and the cavity at 866 nm, both detuned from resonance by an equal amount. Note that for Doppler cooling with the laser at 397 nm, an additional laser at 866 nm must be applied to the ion to avoid trapping of population in the $D_{3/2}$ level.

The $^{40}Ca^{+}$ ion provides a second Λ-system involving the upper $P_{3/2}$ state (see figure 3). It can be used for repumping from the $D_{3/2}$ state, which is connected to the $P_{3/2}$ level by a transition at 850 nm. The state $P_{3/2}$ may decay spontaneously to the state $D_{5/2}$, which has a lifetime of approximately 1 s. We use it to determine the number of $^{40}Ca^{+}$ ions in the cavity by observing quantum jumps in the fluorescence signal. After pumping the ion to the metastable $D_{5/2}$ level, fluorescence at 397 nm is interrupted for an average duration corresponding to the lifetime of the state. The ions decay to the ground state independently, so that the fluorescence intensity returns to its original level in as many steps as there are ions in the trap. If more than one ion is found in this way, their number is reduced by momentarily destabilizing the trap with an additional dc offset applied to the rf electrodes.

We employ a frequency-doubled Ti:sapphire laser for exciting the $S_{1/2} \rightarrow P_{1/2}$ transition. The infrared transitions are driven by grating stabilized diode lasers. All lasers are referenced to an auxiliary diode laser at 852 nm, locked to the D2 line of atomic caesium by means of a scanning Fabry–Perot resonator. In this way, the frequency drift of the lasers is compensated [18].

Residual electric stray fields may be present in the trap, shifting the equilibrium position of the ion off the nodal line of the rf field. Since this would lead to an oscillation of the ion driven by the trapping field (micromotion), radial dc fields must be compensated with correctional voltages applied to the rf electrodes. The optimal ion position is determined by minimizing the Doppler modulation of the fluorescence intensity. Two non-collinear lasers are used for compensating both transverse directions. Displacing the ion along the trap axis, on the other hand, does not lead to micromotion, since the rf fields have no axial components.

The cavity is formed by two mirrors oriented perpendicular to the trap axis and fitting in the horizontal gap between the electrodes (figure 1). The cavity length is stabilized by dithering one of the mirrors at 26 kHz with a piezo, to which an error signal is fed back. This is derived from a photodiode measuring the cavity transmission. Since the intracavity intensity required for a detectable transmission signal strongly saturates the atomic transition, locking and measurements are performed in alternating phases. To this end the locking is periodically interrupted at 437 Hz with a 50% duty cycle by a mechanical chopper. The passive stability of the cavity is sufficient to keep it on resonance during this time. In order to avoid unwanted excitation of the ion, the cooling laser is switched off during the measurement period as well.

As described in section 3, the localization of the ion may be determined with higher precision if short-wavelength fields are used. Consequently, we have employed a cavity on the $S_{1/2} \rightarrow P_{1/2}$ resonance transition in order to determine the position spread of the ion. A sketch of the laser system used in these experiments is presented in figure 4. It shows a probe beam and a chopped locking beam at 397 nm coupled to the cavity, as well as cooling, repumping and shelving beams injected from the side.

3. Deterministic coupling of a single ion to the cavity mode

In order to achieve deterministic control of the ion–cavity coupling, the ion must be localized in the cavity on a scale which is small compared to the structure of the cavity field. In an optical Fabry–Perot resonator, the spatial variation of the atom–field coupling for a Hermite–Gauss mode labelled TEM_{mn} is given by

$$g_{mn}(\vec{r}) = g_0 H_m(\sqrt{2}x/w_0) H_n(\sqrt{2}y/w_0) \mathrm{e}^{-(x^2+y^2)/w_0^2} \cos(2\pi z/\lambda), \tag{1}$$

where the transverse distribution is determined by Hermite polynomials H_m and H_n and the cavity waist w_0.

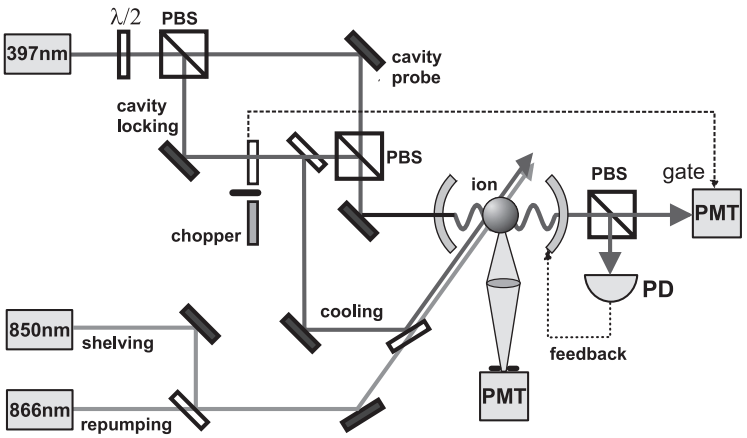

Figure 4. Setup of the laser system used for locking the cavity and exciting and diagnosing the ion coupled to the cavity field. The laser at 850 nm is used for shelving the ion in the $D_{5/2}$ state.

From (1) it is evident that a well-defined coupling requires the ion to be confined in a region of size w_0 in the transverse direction and $\lambda/2$ longitudinally. We have verified that these conditions are actually met in our setup by using the ion as a near-field detector of the field distribution in the cavity [13]. In this way, we have realized an optical probe with atomic-size resolution. Since the ion is freely suspended in the trap, there is no perturbation of the sampled field.

The scans of the cavity field are important for our CQED experiment, not only because they allow us to find the optimum position of the ion in the cavity, but also because the observed resolution provides an upper bound on the localization of the ion. The structured cavity field is used as a ruler to determine the extension of the ion's wavepacket on the relevant scale. The highest precision is reached by using short-wavelength radiation, corresponding to a standing wave with a smaller period. For this reason, we employ a cavity for the 397 nm resonance transition to determine the ion's position spread.

Our cavity has a finesse $F \approx 3000$, a length $L = 6$ mm and mirrors with a radius of curvature $R = 10$ mm, resulting in a cavity linewidth $2\kappa = 8$ MHz and a waist $w_0 = 24\ \mu$m. For the measurement, the cavity field is excited with a weak probe beam (see figure 4), tuned to the $S_{1/2} \rightarrow P_{1/2}$-transition. A particular transverse mode is selected by adjusting the cavity length. The fluorescence is dependent on the local intensity of the mode at the position of the ion. Counting the fluorescence photons as a function of the ion's position therefore yields a map of the mode distribution with a resolution determined by the spread of the ion's wavefunction. As indicated in figure 1, we collect the fluorescent light emitted in the direction of the trap axis (using a lens with numerical aperture 0.17) and detect it with a photomultiplier tube.

Two different techniques are used to precisely position the ion relative to the cavity mode, accommodating our specific experimental conditions. In the direction of the trap axis (x), which coincides with the nodal line of the rf field, the ion itself may be displaced arbitrarily, without exposing it to the delocalizing effect of the alternating trap field. The equilibrium position of the ion along the axis of the trap is shifted by applying slightly different voltages to dc electrodes 4 and 5 (see figures 1 and 2).

Figure 5 shows a scan of the TEM_{30} mode of the cavity obtained in this way. An averaging time of 1 s per point was used. The intensity distribution is not entirely symmetric, because the cavity eigenmodes are slightly displaced and rotated with respect to the trap axis. The inset in figure 5 indicates the path along which the ion is moved. The solid curve in the figure

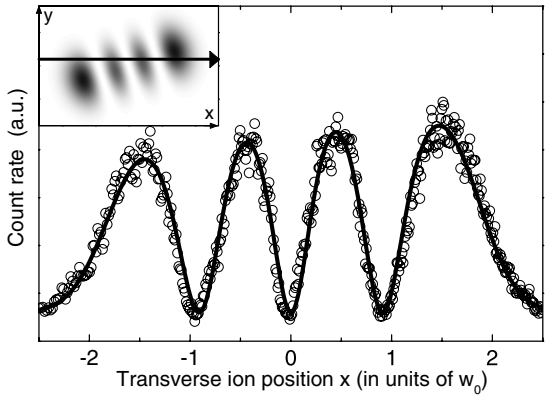

Figure 5. Scan of the TEM_{30} cavity mode along the trap axis. The solid curve is a fit using equation (2). The inset shows the path of the ion through the calculated cavity mode distribution.

represents a fit, taking into account saturation of the ion's transition. From the position-dependent coupling (1), we obtain the following expression for the transverse variation of the fluorescence intensity:

$$I_{\mathrm{fl}}(x, y) = \frac{I_0}{2}\frac{s(x, y)}{1 + s(x, y)}, \qquad s(x, y) = s_0 H_3^2(\sqrt{2}x/w_0)\mathrm{e}^{-2(x^2+y^2)/w_0^2}, \tag{2}$$

with s_0 as the saturation parameter at the centre of the TEM_{00} mode.

In the directions perpendicular to the trap axis (y and z), an alternative technique must be used for positioning the ion in the cavity mode. As discussed above, the reason is the occurrence of micromotion off the trap axis, where the ion is exposed to the rf trapping field. To prevent this, the ion is restrained to the trap axis and the *cavity* is moved instead to access other regions of the field distribution. This is done by piezo-electrically translating the entire cavity assembly. The laser beams for locking and probing the cavity are kept aligned by synchronously tilting a thick glass plate in front of the cavity. An example of a vertical scan of the intensity distribution with the displaced cavity technique is presented in figure 6. Also shown in the figure is a two-dimensional image of the transverse field distribution, obtained by combining the horizontal ion scan with the vertical cavity scan.

The scale of the transverse structure of the cavity field is given by the cavity waist w_0, which is two orders of magnitude larger than the wavepacket of a Doppler-cooled ion. As a consequence, the transverse spread of the ion is not expected to smear out the local coupling constant $g(\vec{r})$. Experimental evidence is given by the perfect correspondence of the measured and calculated intensity distributions in figures 5 and 6.

For the longitudinal direction of the cavity field the situation is more complex, since here the spatial structure (characterized by a standing wave with a period of $\lambda/2$) is comparable in size to the ion's wavepacket. Because the cavity axis is perpendicular to the trap axis, the ion is again kept stationary and the cavity is moved with a piezo-actuator, while monitoring the fluorescence. Figure 7 shows the resulting mapping of one period of the longitudinal field distribution. A sine-wave structure is observed, with a visibility of $V = 40\%$. The limited contrast is due to the width of the ion's wavepacket, exposing it to a finite cavity field even at the node of the intensity distribution. Therefore, the observed visibility is directly linked to

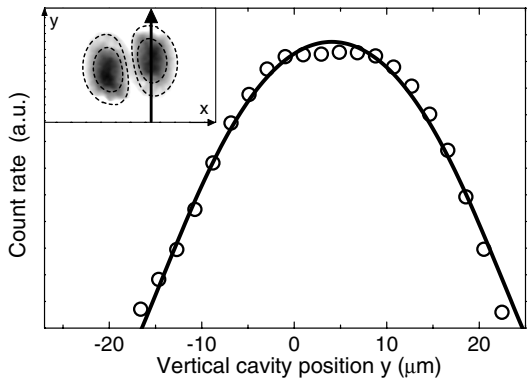

Figure 6. Vertical intensity distribution of the TEM_{10} mode, scanned by displacing the entire cavity. The inset shows a two-dimensional image of the transverse mode distribution, measured by combining the vertical cavity scan with the horizontal ion displacement of figure 5. The arrow indicates the path corresponding to the scan in the main figure.

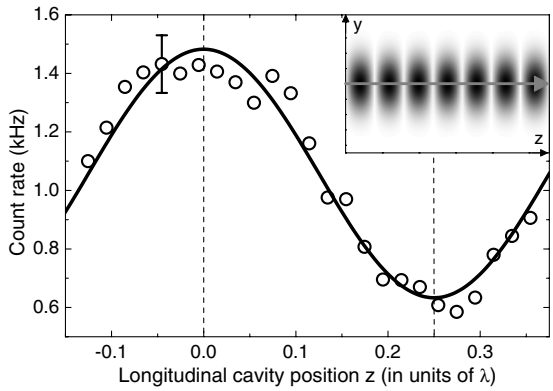

Figure 7. Scan of the longitudinal mode structure. The observed standing wave has a visibility of 40%, corresponding to an ion wavepacket with $a_z = 42$ nm.

the rms position spread $a_z = \sqrt{\langle z^2 \rangle}$ of the ion in the z-direction:

$$V = \exp\{-2(2\pi a_z/\lambda)^2\}. \tag{3}$$

From figure 7, a wavepacket extension $a_z = 42$ nm is derived. This is a factor of 10 lower than the transition wavelength, so that we operate in the Lamb–Dicke regime. The measured wavepacket size corresponds to an ion temperature of 0.5 mK, which is the Doppler-cooling limit for calcium ions. Therefore, it is the thermal spread of the ion's wavefunction which determines the range of coupling values which the ion is exposed to in the cavity field.

Another quantity of interest is the accuracy Δz with which the centroid of the ion's wavefunction is determined. The best localization is obtained at the points with the maximum slope of the standing wave, i.e. at the centre of figure 7:

$$\Delta z \approx \frac{\lambda}{4\pi V\ \mathrm{SNR}}, \tag{4}$$

where a signal-to-noise ratio SNR $\approx$ 5:1, obtained with an integration time of 0.2 s per point, leads to a localization of $\Delta z \approx 16$ nm or $\lambda/25$. This value may be improved by extending the integration time.

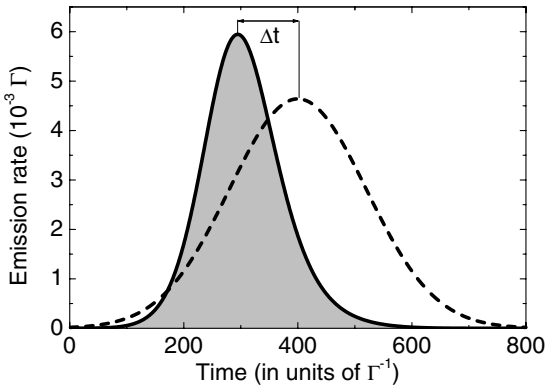

Figure 8. Single-photon pulse (——), obtained with an ion resonantly coupled to the cavity ($g/2\pi = 11.15$ MHz) with ultra-low loss mirrors ($\kappa/2\pi = 446$ kHz). For a peak Rabi frequency $\Omega_0/2\pi = 10.35$ MHz of the resonant pump pulse (- - - -), an efficiency of 98% is predicted. The fixed offset Δt between pump pulse and output pulse corresponds to the triggered emission of the photon. The spontaneous decay rate on the pump transition is $\Gamma/2\pi = 22.3$ MHz.

Combining the measurements of figures 5–7, we obtain a three-dimensional image of the intensity distribution of the cavity field with unprecedented, atomic-scale precision. Conversely, we can realize a precisely defined ion–cavity coupling by placing the ion at a suitable position, determined by relation (1). In most cases, this will be the maximum of the intensity distribution, in order to reach the strong coupling regime. Other applications require a coupling with a specific time dependence $g(t)$, which is realized by displacing the ion along the trap axis (as in the scan of figure 5). The maximum rate of change for the coupling is given by the ion's axial oscillation frequency of a few 100 kHz.

4. Applications of CQED with trapped ions

The deterministic coupling, i.e. the realization of a predefined strength of interaction with the cavity field, which we have demonstrated for a single calcium ion, opens a wide range of applications, which are difficult or impossible to realize with transient atoms. Particularly important for the complete control of the ion–field quantum system is the fact that the coupling may be sustained for an arbitrary period, limited only by the trapping time of the ion, which is several hours.

A goal of fundamental significance is the deterministic generation of triggered single-photon pulses [19]. This can be accomplished by coupling the 866 nm transition to the cavity, while pumping at 397 nm with a coherent field (see figure 3). Starting in the ion's ground state, Raman scattering excites precisely a single photon in the cavity. At the same time, the ion is transferred to the metastable state $D_{3/2}$, so that additional pump photons cannot be scattered into the cavity mode. Due to the finite transmissivity of the cavity mirrors, the photon is transferred to a mode of the free electromagnetic field. This scattering process has been observed with atoms traversing a high-finesse cavity [20]. However, the controlled generation of single photons at arbitrary times requires a stationary atom in the cavity. When a single ion is localized at an antinode of the cavity field, deterministic photon emission with optimum efficiency is ensured.

In figure 8, a numerical solution of the master equation of the ion–cavity system is presented for parameters attainable in our experiment. In response to a Gaussian pump pulse $\Omega(t)$, a single photon is emitted from the cavity with 98% efficiency. In the remaining cases

either no excitation occurs, or an infrared photon is scattered as fluorescent light to a mode outside the cavity. Figure 8 shows that the peak of the single-photon pulse occurs at a well-defined time before the peak of the pump pulse. Likewise, the shape of the single-photon pulse is controlled by the pump pulse. An important property of the output pulse is its spectral composition. A calculation of the pulse spectrum shows that it is Fourier limited, which is of great importance for applications in quantum information processing.

In the linear ion trap we have also stored strings of ions along the trap axis, with equilibrium positions determined by the Coulomb repulsion. The internal states of the ions may be used as a register in a prospective quantum computer [21]. While there is no direct coupling between them, adjacent ions in the chain may exchange quantum information through the cavity mode [22–24]. This is a viable alternative to the vibrational coupling of ionic qubits [21, 25, 26]. To test the feasibility of this scheme, we have repeated the mode mapping experiments with a two-ion crystal, displaced in the direction of the trap axis. The fluorescence data we obtained showed the same resolution as in the case of a single ion. For the strongest interaction, we adjusted the ion separation to couple the ion pair to the peaks of the TEM_{10} mode. In the same way, two adjacent ions in a long chain can be selectively coupled to the cavity.

The cavity not only provides an interface between ions and photons. By coupling the cavity to a vibrational sideband of the ion motion in the trap [27], motional states generated in an ion string may be swapped to the photon field [28]. This has promising applications in the generation of non-classical photon states. Thus, CQED with ions is a versatile tool of central importance for the generation and manipulation of the quantum states of atoms and photons.

References

[1] Berman P R (ed) 1994 Cavity quantum electrodynamics *Advances in Atomic, Molecular and Optical Physics* Suppl. 2 (San Diego, CA: Academic)
[2] Varcoe B T H, Brattke S, Weidinger M and Walther H 2000 *Nature* **403** 743
[3] Rempe G and Walther H 1987 *Phys. Rev. Lett.* **58** 353
[4] Rempe G, Thompson R J, Brecha R J, Lee W D and Kimble H J 1991 *Phys. Rev. Lett.* **67** 1727
[5] Thompson R J, Rempe G and Kimble H J 1992 *Phys. Rev. Lett.* **68** 1132
[6] Monroe C 2002 *Nature* **416** 238
[7] Turchette Q A, Hood C J, Lange W, Mabuchi H and Kimble H J 1995 *Phys. Rev. Lett.* **75** 4710
[8] van Enk S J, Cirac J I and Zoller P 1997 *Phys. Rev. Lett.* **78** 4293
[9] Cirac J I, Zoller P, Kimble H J and Mabuchi H 1997 *Phys. Rev. Lett.* **78** 3221
[10] Hood C J, Lynn T W, Doherty A C, Parkins A S and Kimble H J 2000 *Science* **287** 1447
[11] Pinkse P W H, Fischer T, Maunz P and Rempe G 2000 *Nature* **404** 365
[12] Gosh P K 1995 *Ion Traps* (Oxford: Clarendon)
[13] Guthöhrlein G R, Keller M, Hayasaka K, Lange W and Walther H 2001 *Nature* **414** 49
[14] Kjærgaard N, Hornekær L, Thommesen A M, Videsen Z and Drewsen M 2000 *Appl. Phys.* B **71** 207
[15] Gulde S, Rotter D, Barton P, Schmidt-Kaler F, Blatt R and Hogervorst W 2001 *Appl. Phys.* B **73** 861
[16] Rempe G, Thompson R J, Kimble H J and Lalezari R 1992 *Opt. Lett.* **17** 363
[17] Hood C J, Kimble H J and Ye J 2001 *Phys. Rev.* A **64** 033804
[18] Zhao W Z, Simsarian J E, Orozco L A and Sprouse G D 1998 *Rev. Sci. Instrum.* **69** 3737
[19] Law C K and Kimble H J 1997 *J. Mod. Opt.* **44** 2067
[20] Kuhn A, Hennrich M and Rempe G 2002 *Phys. Rev. Lett.* **89** 067901
[21] Cirac J I and Zoller P 1995 *Phys. Rev. Lett.* **74** 4091
[22] Pellizzari T, Gardiner S A, Cirac J I and Zoller P 1995 *Phys. Rev. Lett.* **75** 3788
[23] Zheng S B and Guo G C 2000 *Phys. Rev. Lett.* **85** 2392
[24] Shahriar M S, Bowers J A, Demsky B, Bhatia P S, Lloyd S, Hemmer P R and Craig A E 2001 *Opt. Commun.* **195** 411
[25] Monroe C, Meekhof D M, King B E, Itano W M and Wineland D J 1995 *Phys. Rev. Lett.* **75** 4714
[26] Sackett C A *et al* 2000 *Nature* **404** 256
[27] Mundt A B, Kreuter A, Becher C, Leibfried D, Eschner J, Schmidt-Kaler F and Blatt R 2002 *Phys. Rev. Lett.* **89** 103001
[28] Parkins A S and Kimble H J 1999 *J. Opt. B: Quantum Semiclass. Opt.* **1** 496